How to cite: *Angew. Chem. Int. Ed.* **2021**, *60*, 16109–16118
International Edition: doi.org/10.1002/anie.202104223
German Edition: doi.org/10.1002/ange.202104223

Fullerenes

An Ultra-Long-Lived Triplet Excited State in Water at Room Temperature: Insights on the Molecular Design of Tridecafullerenes

Javier Ramos-Soriano, Alfonso Pérez-Sánchez, Sergio Ramírez-Barroso, Beatriz M. Illescas, Khalid Azmani, Antonio Rodríguez-Fortea, Josep M. Poblet, Cormac Hally, Santi Nonell, David García-Fresnadillo,* Javier Rojo, and Nazario Martín**

Abstract: *Suitably engineered molecular systems exhibiting triplet excited states with very long lifetimes are important for high-end applications in nonlinear optics, photocatalysis, or biomedicine. We report the finding of an ultra-long-lived triplet state with a mean lifetime of 93 ms in an aqueous phase at room temperature, measured for a globular tridecafullerene with a highly compact glycodendrimeric structure. A series of three tridecafullerenes bearing different glycodendrons and spacers to the C_{60} units have been synthesized and characterized. UV/Vis spectra and DLS experiments confirm their aggregation in water. Steady-state and time-resolved fluorescence experiments suggest a different degree of inner solvation of the multifullerenes depending on their molecular design. Efficient quenching of the triplet states by O_2 but not by waterborne azide anions has been observed. Molecular modelling reveals dissimilar access of the aqueous phase to the internal structure of the tridecafullerenes, differently shielded by the glycodendrimeric shell.*

Introduction

Fullerenes, their multi-adduct derivatives and many other carbon-based nanometric-size related species have been proposed as valuable key nanomaterials in different fields such as optoelectronics, photovoltaics, photocatalysis or biomedicine.[1] Organization of these materials at the nanoscale may play a significant role in their performance, since the way how the nanomaterial is intra-/intermolecularly assembled can be of paramount importance in phenomena such as energy/electron transfer, supramolecular interactions, solvation, or for the delivery of species, when the processes are considered at small length scales.[2]

A common strategy for the development of applications based on [60]fullerene is the design of multi-adduct derivatives with appropriate substituents imparting good solubility and intra-/intermolecular interactions for the desired purpose.[3] Hexakis-adducts of C_{60} are suitable scaffolds for the construction of giant molecules (e.g. tridecafullerenes or carbon nanotube-fullerene conjugates) with promising applications,[4] whose structural implications and photophysical properties, however, have not been completely unravelled yet.

Sugar residues surrounding the hydrophobic C_{60} core allow excellent solubility of these derivatives in polar solvents like water. Thus, the 1:2 [60]fullerene-γ-cyclodextrin host-guest complex was shown to preserve the fullerene's ability to photosensitize the production of singlet oxygen (hereafter $^1O_2$) despite a ca. 50% reduction of the fullerene surface accessible to oxygen from the aqueous phase, owing to the effective shielding by the two cyclodextrin moieties.[5] However, in the case of glycodendro[60]fullerene monoadducts, their amphiphilic behavior can cause self-assembly in water (favoured through π-π interactions between the C_{60} moieties), leading to formation of well-defined compact micellar supramolecular aggregates.[6] Mannose-derivatized conjugates have been widely applied as recognition elements or labelling agents of biological substrates,[7] as key components of sensors,[8] in fluorescence imaging,[9] and in the photodynamic therapy of pathogens[10] or cancer.[11]

Herein we report on the synthesis, structural and photophysical characterization in water and molecular modelling of

[*] Dr. J. Ramos-Soriano, Dr. A. Pérez-Sánchez, S. Ramírez-Barroso, Prof. B. M. Illescas, Prof. D. García-Fresnadillo, Prof. N. Martín
Department of Organic Chemistry, Faculty of Chemistry, University Complutense of Madrid
Avenida Complutense, 28040 Madrid (Spain)
E-mail: beti@ucm.es
dgfresna@ucm.es
nazmar@ucm.es
K. Azmani, Dr. A. Rodríguez-Fortea, Prof. J. M. Poblet
Department of Physical and Inorganic Chemistry, Rovira i Virgili University
Marcel lí Domingo 1, 43007 Tarragona (Spain)
Dr. C. Hally, Prof. S. Nonell
Institut Químic de Sarrià, Universitat Ramon Llull
Via Augusta 390, 08017 Barcelona (Spain)
Dr. J. Rojo
Glycosystems Laboratory, —Chemical Research Institute (IIQ)
CSIC—Seville University
Avenida Américo Vespucio 49, 41092 Sevilla (Spain)
Prof. N. Martín
IMDEA Nanoscience Institute
C/ Faraday 9, Campus de Cantoblanco, 28049 Madrid (Spain)
Supporting information and the ORCID identification number(s) for the author(s) of this article can be found under: https://doi.org/10.1002/anie.202104223.

a series of globular glycodendrimeric tridecafullerenes decorated with mannose sugars as terminal units (**11**–**13**, Scheme 1 and Scheme 2). These globular multifullerenes display rather long-lived triplet excited states and, in particular, compound **13** shows an exceptionally long mean triplet lifetime of 93 ms in aqueous phase at room temperature. This experimental finding has no precedents in the previous literature, since this value is in sharp contrast with the other much shorter-lived fullerene derivatives under study in this article. Moreover, the ultra-long-lived triplet excited state of compound **13** measured in this work is also well apart from those triplet lifetimes described for other organic molecules or coordination compounds, in solution at ambient temperature, reported so far.[12]

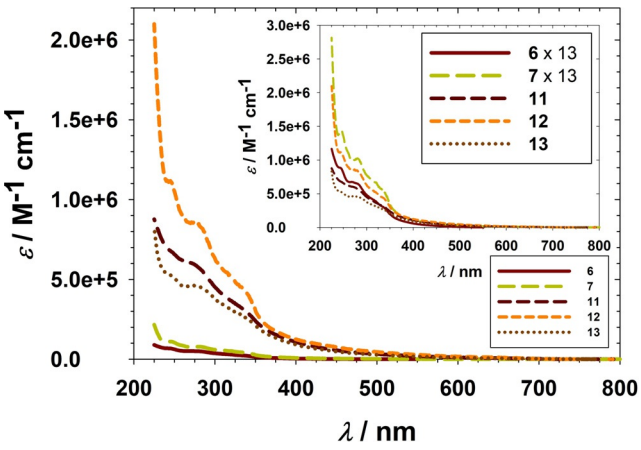

Figure 1. UV/Vis absorption spectra (phosphate saline buffer, PBS solution, pH 7.4) of the mannose-labelled tridecafullerenes **11**–**13** under study and their corresponding hexakis-adduct structural precursors **6** and **7**.

Results and Discussion

Synthesis and Characterization

The synthesis of tridecafullerenes **11** and **12** was carried out by following a click-chemistry based synthetic strategy as depicted in Scheme 1. From monoadduct **1**, hexakis-adduct **3** was obtained by Bingel-Hirsch cycloaddition of di(pent-4-yn-1-yl) malonate,[13] yielding the asymmetric derivative appended with ten alkyne moieties and a chloride group at the focal point. Addition of the carbohydrate azides **4** or **5** by copper-catalyzed azide-alkyne cycloaddition (CuAAC)[14] in DMSO, using $CuBr{\cdot}S(Me)_2$ as catalyst,[15] leads to the chloride derivatives **6** and **7** which, after treatment with sodium azide, allow the quantitative preparation of the building blocks **8** and **9** appended with 10 and 30 sugar moieties, respectively. From these azide fullerene hexakis-adducts, tridecafullerenes **11** and **12** can be obtained by CuAAC click chemistry reaction with symmetric alkyne derivative **10**.[16] Compounds **11** and **12** are endowed with 120 and 360 mannose units, respectively, and were obtained in 83% and 58% yield after purification by ultrafiltration (Amicon®). The synthesis and characterization of tridecafullerene **13** (Scheme 2) has been reported elsewhere.[4d] Characterization of all new compounds and their aggregation in water (Figure S1) was carried out by using standard techniques (Supporting Information).

Photophysical Characterization

The absorption spectra of tridecafullerenes **11**–**13** and their hexakis-adduct structural precursors **6** and **7** in PBS solution are depicted in Figure 1 and S2. The UV/Vis spectral features are collected in Table 1 and are in good agreement with previous reports of hexakis-adducts with relatively similar substitution patterns.[17]

A remarkable hypochromic shift was observed in the UV/Vis absorption spectra of tridecafullerenes **11**–**13** when the absorption coefficients of the peaks in the 269–273 nm region were compared with those of their respective hexakis-adduct precursors × 13 (Figure 1 insert).[18] Hypochromicities were in the 10–15% range for **11** vs. **6** and **12** vs. **7**, respectively, while a 30% hypochromic shift was observed in the case of **13** vs. **6**. Such a hypochromic effect could be related to solvent exclusion in the case of tridecafullerenes, due to their more compact structure vs. the hexakis-adduct precursors, favouring hydrophobic interactions in the inner domain, and to their tendency to self-aggregate via supramolecular interactions by

Table 1: Structural features and optical absorption parameters of the mannose-labelled tridecafullerenes **11**–**13** under study and their corresponding hexakis-adduct structural precursors **6** and **7** (shell units of C_{60}).[a]

Compound	C_{60} units		Spacers		Sugars	UV/Vis absorption
	core	shell	C_{60}-C_{60}	C_{60}-sugar		λ_{abs}^{max} [nm][b] (ε [$mol^{-1}\,dm^3\,cm^{-1}$])[c]
6	0	1	0	A	10	214 (107500), 241 sh (68400), 269 (52000), 276 sh (50600), 313 sh (32100), 335 sh (23600)
11	1	12	I	A	120	213 (1084600), 247 sh (672400), 269 sh (603900), 330 sh (332600)
7	0	1	0	B	30	211 sh (349200), 245 (110600), 280 (78800), 309 sh (55100), 320 sh (51300), 332 sh (44100)
12	1	12	I	B	360	243 (1119000), 273 (859000), 316 sh (539400), 332 sh (453300)
13	1	12	II	A	120	244 sh (529200), 272 (463700), 309 sh (341800), 321 sh (308700), 331 sh (283000)

[a] The structural features are defined according to the number of [60]fullerene hexakis-adduct units (at the core and/or shell, only shell units are considered in the case of the synthetic precursors **6** and **7**), on the type of spacer units between the core–shell fullerenes and the shell fullerene-terminal sugar (mannose), and on the number of terminal sugars at the distal ends of the shell fullerenes, according to Schemes 1 and 2, as follows: core fullerene **10**, shell fullerenes **6** or **7**, spacer I = CH_2-$(CH_2OCH_2)_3$-CH_2O-$(CH_2)_4$; spacer II = $(CH_2)_6$; spacer A = $(CH_2)_3$-(1,2,3-triazole)-$(CH_2)_2$-O-mannose (α); spacer B = $(CH_2)_3$-(1,2,3-triazole)-(CH_2)-$(CH_2OCH_2)_4$-C-[CH_2OCH_2-(1,2,3-triazole)-$(CH_2)_2$-O-mannose (α)]$_3$. [b] PBS aqueous solution, pH 7.4. Wavelength uncertainty ±3 nm for peaks, ±5 nm for shoulders (sh). [c] Uncertainty ±15%.

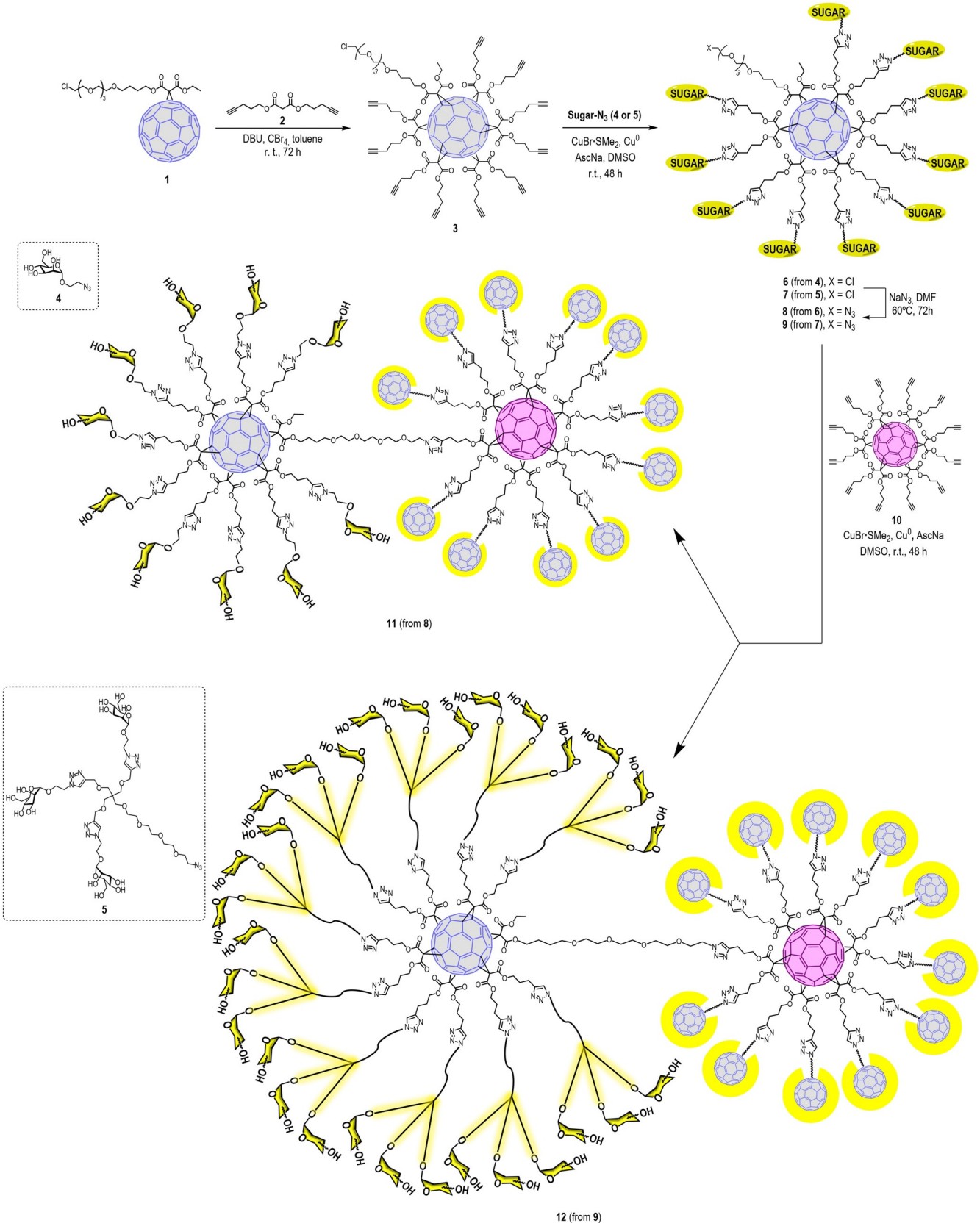

Scheme 1. Synthesis of tridecafullerenes **11** and **12**.

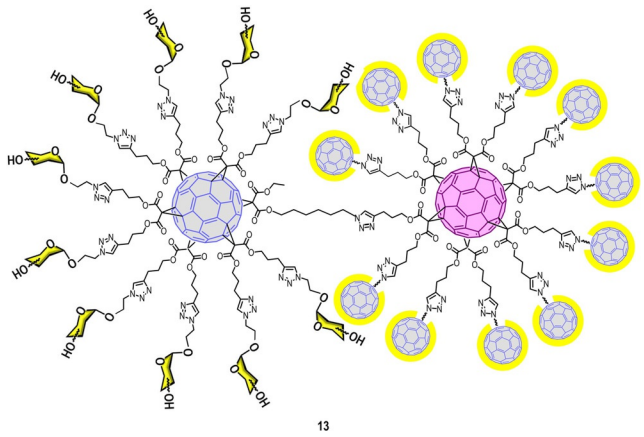

Scheme 2. Structure of tridecafullerene **13**.

hydrogen bonding between the external sugar residues (Figure S1). To some extent, this hypochromism would be similar to the changes in optical density observed when nucleobase interactions are modified in nucleic acids, due to changes in solvent composition or during melting/annealing processes.[19]

Table 2 collects the wavelengths of the fluorescence emission maxima (λ_{em}^{max}) and the lifetimes of the singlet (τ_S) and triplet (τ_T) excited states of tridecafullerenes **11–13** and their corresponding hexakis-adduct structural precursors, **6** for **11** and **13**, and **7** for **12**. Table 2 also collects the dynamic bimolecular quenching rate constant of the lowest triplet excited states (T_1) by O_2 ($k_q^{T_{O_2}}$), the probability of T_1 quenching by molecular oxygen ($P^{T_{O_2}}$), and the singlet oxygen production quantum yield (Φ_Δ) and $^1O_2$ lifetime (τ_Δ) in PBS solution.

A blue shift about 15 nm between λ_{em}^{max} of **6** and **7** is observed (compare spacer A for **6** vs. spacer B for **7** with a larger glycodendrimeric structure and number of sugar units). Tridecafullerenes **11–13** also show blue-shifted emission with respect to their respective monofullerene precursors **6** and **7** (Figure S3). In particular, compound **13** shows a 134 nm shift with respect to **6**. These results agree with the hypothesis of decreased solvation illustrated by the hypochromic shift of absorption spectra of tridecafullerenes, especially **13**, evidencing a poorer stabilization of the excited singlet state due to less water solvation in the tridecafullerenes.

Moreover, the nanoheterogeneous behavior of these systems is supported by the bi-exponential functions usually required to fit the fluorescence decays (Figure S4). Furthermore, the mean emission lifetimes (τ_{SM}) are shorter in **11–13** than in **6** and **7**, showing that S_1 is less stabilized in the case of the tridecafullerenes due to reduced interactions with the polar solvent, as confirmed by the higher energy gap of **11–13**. Compound **13** shows again an extreme behavior, displaying the shortest fluorescence lifetime (0.22 ns) and highest energy gap.

Concerning the T_1 lifetime in the absence of quenchers (τ_{T_0}), longer lifetimes are shown by tridecafullerenes **11–13** in comparison with **6** and **7** (both displaying lifetimes around 50 μs). Almost a twofold increase from 64 to 110 μs can be observed when **11** and **12** are compared (cf. spacer A vs. spacer B with a larger glycodendrimeric structure, Table 1, Scheme 1 and Scheme 2). Furthermore, in the case of compound **13**, an extraordinarily long triplet mean lifetime (τ_{TM}) of 93 ms was detected, whose discrete components τ_1 and τ_2 are 30 ms (42% amplitude) and 280 ms (58% amplitude), respectively (Table 2, Figure 2 and S5).

According to previous literature reports on the photophysics of [60]fullerene-sugar conjugates (Bingel-type monoadducts), these derivatives show shorter T_1 lifetimes on going from hydrophobic to polar environments (ca. 50 μs in toluene vs. 35 μs in acetonitrile),[22] providing additional support to the hypothesis suggesting lower polarity around the C_{60} units of the globular tridecafullerenes vs. the more open monofullerenic hexakis-adduct precursors **6** and **7**, due to limited solvent accessibility to the inner domains of **11–13**. Moreover, when

Table 2: Photophysical parameters of the mannose-labelled tridecafullerenes **11–13** under study and their corresponding hexakis-adduct structural precursors **6** and **7**.[a]

Compound	λ_{em}^{max} [nm][b]	τ_S [ns] (% amplitude)[c] τ_1	τ_2	τ_{SM}[j]	τ_{T_0} [μs][d]	τ_{Tair} [μs][e]	$k_q^{T_{O_2}}$ [$M^{-1}s^{-1}$][f]	$P^{T_{O_2}}$[g]	Φ_Δ[h]	τ_Δ [μs][i]
6	652	1.0 (77)	3.1 (23)	1.5	50	2.7	1.30×10^9	0.95	0.11	66.2
11	590	0.5 (74)	2.7 (26)	1.1	64	4.2	0.82×10^9	0.93	0.02	63.5
7	635	1.1 (84)	4.1 (16)	1.6	53	4.4	0.77×10^9	0.92	0.13	63.0
12	616	0.5 (66)	3.0 (34)	1.3	110	9.1	0.37×10^9	0.92	0.05	64.6 3.7[l]
13	518	0.2 (97)	2.5 (3)	0.22	τ_1 30000[k] τ_2 280000[k] τ_{TM} 93000[j]	0.42	8.50×10^9	0.99	0.07	3.2[l]

[a] PBS aqueous solution, pH 7.4. [b] Wavelength uncertainty ±10 nm. [c] Singlet excited state lifetime, biexponential fitting of the time-dependent fluorescence intensity decay profiles was usually required ($I_F(t)=A+\Sigma B_i\times e^{(-t/\tau_i)}$, $i=1, 2$) where B_i is the corresponding preexponential factor related to signal amplitude and τ_i is the discrete lifetime component. Uncertainty ±10%. [d] Triplet excited state lifetime in the absence of quencher. Ar-purged deuterated PBS solution. Uncertainty ±10%. [e] Triplet excited state lifetime in the presence of O_2 quencher. Air-equilibrated d-PBS solution. Uncertainty ±10%. [f] Dynamic bimolecular quenching rate constant of triplet excited states by O_2. Uncertainty ±15%. [g] Probability of triplet excited state quenching by O_2 under air-equilibrated conditions. $P^{T_{O_2}}=1-(\tau_{T_{air}}/\tau_{T_0})$. [h] Singlet oxygen production quantum yield. Uncertainty ±10%. [i] Singlet oxygen phosphorescence lifetime measured in d-PBS solution with an optical density ≤0.1 at 355 nm (dye concentrations in the 10^{-5}–10^{-6} M range) in very good agreement with the expected $^1O_2$ lifetime in deuterium oxide, 64.4 μs.[20] Uncertainty ±3%. [j] τ_M is the preexponential weighted mean lifetime ($\tau_M=\Sigma B_i\times\tau_i/\Sigma B_i$), where τ_{SM} and τ_{TM} stand for the mean lifetime of the singlet and triplet excited states, respectively.[21] Uncertainty ±10%. [k] Biexponential fitting of the triplet excited state decay profile was required. [l] Singlet oxygen lifetime in PBS solution.

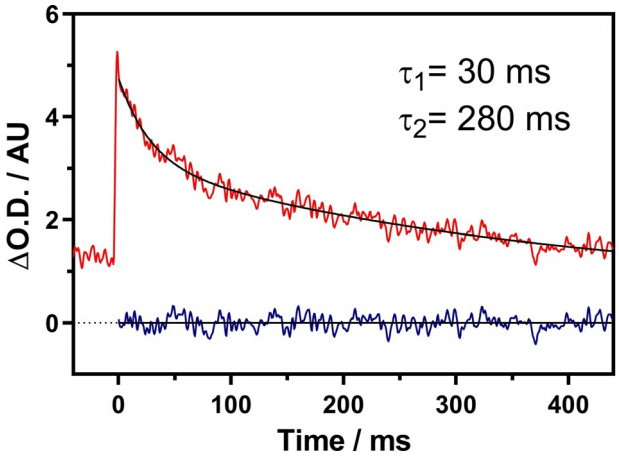

Figure 2. Red line: Transient absorption of the triplet excited-state of **13** in Ar-purged deuterated PBS (λ_{exc} 355 nm, λ_{obs} 650 nm, 9.4 mJ pulse^{-1}). Black line: Fit of a biexponential decay function to the data. Blue: Residuals plot.

the series **11**–**13** is considered, tridecafullerene **13** is the one showing the longest triplet lifetime (93 ms) and the highest hypochromic shift in the UV/Vis absorption spectrum. It also shows the largest blue-shifted fluorescence and shortest lived S_1. These differences in the photophysical properties of **13** may be attributed to the fact that compound **13** has got spacer II (hydrophobic shorter alkyl) vs. I (hydrophilic longer polyether) when **13** and **11**, with the same A spacer and number of sugar units, are compared.

It has to be noted that such a long triplet lifetime has never been described for a fullerene derivative at room temperature in the liquid phase. In this way, a triplet lifetime of 0.25 ms for pristine C_{60} in benzene-like solvents has been reported,[12a] while lifetimes in the 0.4–55 ms range have only been reported for C_{60} in the solid phase (either for crystalline C_{60} or in glass or rare gas matrices at 1–10 K, 0.4 ms; or in C_{60} thin films, 55 ms)[23] and lifetimes below 0.30 ms have been described for multi-adduct blends of fullerenes for organic solar cells.[24] Concerning [60]fullerene hexaadducts, phosphorescence lifetimes of 4.4 and 3.7 s have singularly been reported for two hexapyrrolidine derivatives of C_{60} with T_h and D_3 symmetry, respectively, at 77 K, again in a glass matrix.[25] In fact, to the best of our knowledge, such an exceptionally long-lived triplet state has never been described in the previous literature on photophysics of organic molecules or coordination compounds in solution at room temperature.[12] Long T_1 lifetimes are of particular interest in applications like photocatalysis, photovoltaics, biomedicine and optoelectronics based on nonlinear phenomena.

Concerning quenching by molecular oxygen, the T_1 lifetimes of the air-equilibrated aqueous solutions (τ_{Tair}) are in the 0.4–9.1 μs range (cf. 0.29 μs for C_{60} in toluene),[26] and allowed the determination of the dynamic bimolecular quenching rate constants by O_2 ($k_q{}^T{}_{O_2}$, Table 2) via Stern–Volmer analysis (Supporting Information). The observed $k_q{}^T{}_{O_2}$ are ca. one order of magnitude below the theoretical diffusion control limit in water at 25 °C (Smoluchowski's theory, $k_{qdiff}{}^T \approx 7.4\times10^9$ M^{-1} s^{-1}),[27] except for **13** (with spacer II vs. I), and are higher for the series **11** vs. **12** and **6** vs. **7** when spacer A vs. B is concerned and the precursor hexakis-adducts or their corresponding tridecafullerenes are also compared, revealing the consequences of the molecular design. In this way, tridecafullerene **12**, the only one with three-branched terminal sugar units (Scheme 1), which should show the most entangled sugar shell, as described in the Computational Analysis section, is the tridecafullerene with the lowest bimolecular quenching constant by dioxygen (0.37×10^9 M^{-1} s^{-1}). This trend is also followed by compound **7**, its structural precursor (0.77×10^9 M^{-1} s^{-1}, Table 2) thus revealing a higher steric hindrance towards O_2 difussion. Conversely, and once again, the behavior of compound **13** is specific, since the bimolecular quenching rate constant by O_2 (8.5×10^9 M^{-1} s^{-1}) is purely diffusion-controlled given the excellent agreement, within experimental error (±15%), with the theoretical $k_{qdiff}{}^T$ rate constant.

Regarding the probability of T_1 quenching by O_2 ($P^T{}_{O_2}$), rather high values (>92%, Table 2) have been observed in all cases under air-equilibrated conditions, according to the long lifetimes of the triplet states providing enough time for the quencher-quenchee encounter to occur. Indeed, compound **13** deserves a special comment again, since its unprecedented long τ_{T_0} allows for the quantitative quenching of its T_1 state by O_2.

A study of the $^1O_2$ production quantum yield (Φ_Δ) by these compounds sheds light on the efficiency of the intersystem crossing process generating T_1, since Φ_Δ is limited by the value of the triplet state quantum yield (Φ_T, $\Phi_\Delta \leq \Phi_T$).[28] The Φ_Δ values of the hexakis-adducts **6** and **7** (0.11 and 0.13, respectively) are, within experimental error, in excellent agreement with the Φ_Δ and Φ_T values that can be expected for Bingel-Hirsch-type hexakis-adducts (0.11 for Φ_T).[17e] On the other hand, the Φ_Δ values of tridecafullerenes **11**–**13** are well below the 0.11 limit of Φ_T for the hexakis-adduct building block, and show strong differences between them (Table 2). This could also be explained by a different solvent access to the tridecafullerene's core, consequently influencing, via changes in the polarity around the fullerene units, the Φ_T value, the stability of T_1, and its τ_{T_0}. Indeed, several properties of tridecafullerenes **11**–**13** such as the UV/Vis hypochromic effect, the presence of aggregates (Figure S1),[4d] the blue-shifted emission and shorter fluorescence lifetimes, the increase of τ_{T_0} from **6**, **7** to **11**–**13** and, moreover, the dependency of the Φ_T of C_{60} with the polarity of the medium (0.80 in long-chain alkanes vs. 1.0 in benzene),[29] point to a solvent effect influencing Φ_T of the tridecafullerenes. Therefore, water exclusion from **11**–**13**, by comparison with their hexakis-adduct precursors **6** and **7**, seems to be of paramount importance concerning the properties of tridecafullerenes (see also the Computational Analysis section).

In order to gain deeper insight into the role played by the aqueous solvent and its possible exclusion from the inner domains of the tridecafullerenes, the ability of sodium azide to quench the T_1 of **13** was examined in deuterated PBS. Compound **13** is ideal for this experiment because its ultra-long T_1 lifetime provides the highest sensitivity for probing its own microenvironment. On the other hand, azide anion (N_3^-) is able to deactivate triplet excited states efficiently through

energy/electron transfer processes.[30] However, unlike molecular oxygen, the azide anion must be transported by the solvent to the close environment of the excited state in order to deactivate it. Therefore, quenching of T_1 of **13** by N_3^- should be dependent on the access of water, as a carrier of azide anions, to the C_{60} units inside the globular structure of the tridecafullerene.

Stern–Volmer analysis of quenching experiments of T_1 of **13** by azide yielded a dynamic bimolecular quenching rate constant ($k_{q\ azide}^{T}$) of $2.5(\pm 0.5)\times 10^4\ M^{-1}s^{-1}$ (Figure S6), well below the diffusion control limit expected in water (k_{qdiff}^{T}). Furthermore, the decay traces of T_1 of **13** show a noticeable decrease of the signal amplitudes at zero time as the quencher concentration increases (Figure S6). This result could be explained if a fraction of those T_1 states of **13** reached by N_3^- could be statically quenched. Accordingly, a value of $1.1(\pm 0.3)\times 10^4\ M^{-1}$ was found for the equilibrium constant for complex formation between **13** and sodium azide (Figure S6). Recently, weak binding interactions between NaN_3 and C_{60} have been evidenced by ^{14}N NMR experiments.[31] In this regard, formation of a yellow complex between N_3^- and **13** has been detected by UV/Vis spectroscopy (Figure 3). A

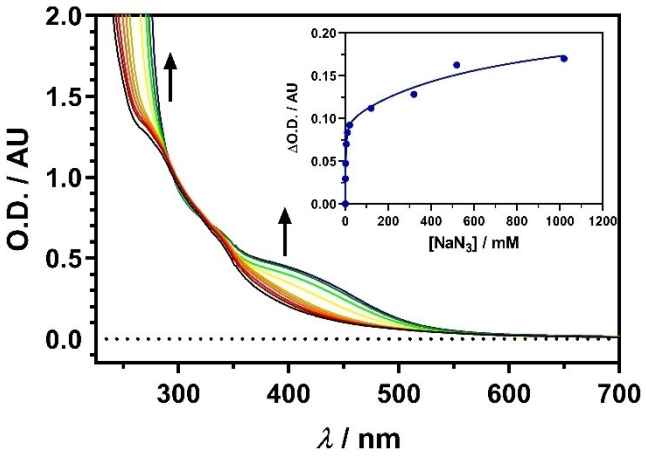

Figure 3. Changes in the UV/Vis absorption spectrum of **13** ([**13**] = 2 μM) upon addition of azide anion from 0 mM (black) to 1020 mM (blue). Insert shows the fit of a dual 1:1 and 1:2 complex formation model between **13** and azide anion to the absorbance data at 366 nm (see also Figure S7).

Benesi–Hildebrand plot revealed a deviation of linearity at high concentrations of N_3^- (not shown), suggesting that a second azide ion binds to the initial complex. Indeed, the optical density difference ($\Delta O.D. = O.D.(\mathbf{13} + N_3^-) - O.D.(\mathbf{13})$, Figure S7) shows a maximum that shifts to longer wavelengths with increasing N_3^- concentrations, suggesting the formation of two complexes. The data could be fitted satisfactorily (Figure 3) with a model where a 1:1 complex is initially formed, which binds a second azide ion at higher concentrations. The fit yielded the 1:1 and 1:2 complex formation constants of 741 M^{-1} and 2.2 M^{-1}, respectively. The much lower value of the second constant is consistent with the hindrance of a second N_3^- incorporation by the higher electrostatic barrier around the fullerene.

Computational Analysis

Theoretical calculations in simplified model systems were performed in order to describe the most characteristic structural features of these glycodendrimeric multifullerenes. Due to the high complexity of **11**–**13**, we started our study with the central (core) [60]fullerene (Supporting Information, Table S1 and Figure S8) and then increased the complexity step by step to the peripheral fullerenes and from the peripheral fullerenes to the final tridecafullerene (see the SI and Figures S9-S12 for more details).

The models made by three C_{60} fullerenes show that the longer the C_{60}-C_{60} spacer, I vs. II, the higher the distance between the peripheral fullerenes (d_1) and the higher the α angle. In general, isosceles triangle dispositions are reproduced, i.e., the pairs of values for the d_2 distance and the β angle are very similar (Figure 4, S9 and Table 3).

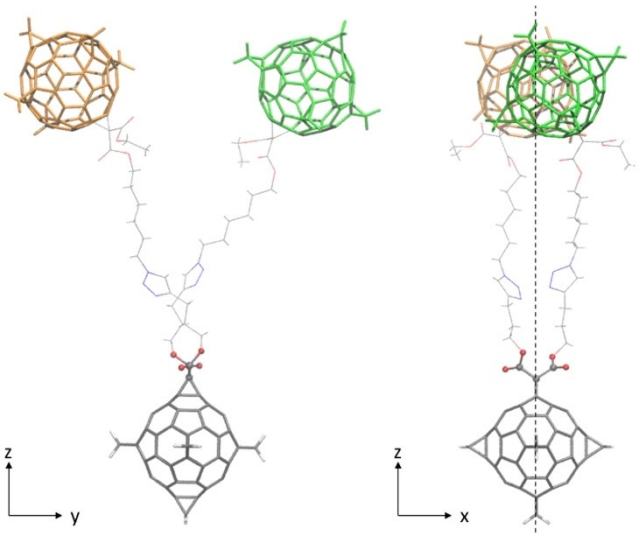

Figure 4. Two views of the optimized structure for the simplest model of three C_{60} of the glycofullerene with spacer II. In this model $\mathbf{M_{II}}$, the peripheral fullerenes are not functionalized with sugars. The three fullerenes define, roughly, an isosceles triangle characterized by d_1 (distance between the centre of mass of the two peripheral fullerenes -brown and green-), d_2 (distance from the centre of mass of one peripheral fullerene to the core fullerene -grey-), α (angle between the peripheral-core-peripheral fullerenes) and β (angles between the peripheral-peripheral-core fullerenes (Figure S9).

When the models are functionalized with the external carbohydrates we observe that there is a non-negligible interaction between the peripheral fullerenes because the distances between them (d_1) decrease with respect to non-functionalized systems ($\mathbf{M_I}$ and $\mathbf{M_{II}}$). This fact is corroborated by the interaction energies calculated considering only the two peripheral fullerenes (what we call "Two C_{60}" model in Table 3), where the spacer to the core fullerene was removed. In the two C_{60} model, the structures for $\mathbf{M_{IA}}$, $\mathbf{M_{IB}}$ and $\mathbf{M_{IIA}}$ were re-optimized, but the variation in the d_1 distance is hardly changed with respect to those obtained in the anchored three C_{60} model. The computed interaction energies are significantly different from zero, with values ranging between

Table 3: Geometrical parameters and interaction energies for models made by three and two C_{60} fullerene.

Model[a]	Spacers		Compound	Three C_{60} model				Two C_{60} model[d]		
	C_{60}–C_{60}	C_{60}–sugar		d_1 [Å]	d_2 [Å]	α [°]	β [°]	d_1 [Å]	E (PM6)[e]	E (DFT)[f]
M_I	I	CH_2[b]		31.3	38.5 | 38.6	47.9	66.1 | 65.9	31.3	0.0	0.0
M_{IA}	I	A	**11** (52.0 Å)[c]	27.8	34.8 | 34.2	47.5	65.1 | 67.3	27.8	−39.8	−59.8
M_{IB}	I	B	**12** (71.1 Å)[c]	31.1	35.9 | 35.9	47.0	64.3 | 64.4	31.1	−94.5	–
M_{II}	II	CH_2[b]		17.4	27.5 | 27.8	36.8	70.7 | 72.5	17.4	0.0	0.0
M_{IIA}	II	A	**13** (42.3 Å)[c]	15.7	25.5 | 26.6	35.0	68.9 | 76.1	14.5	−71.8	−115.0

[a] Model systems are defined considering spacers as defined in Table 1 (see also the SI). $\mathbf{M_{IA}}$, $\mathbf{M_{IB}}$ and $\mathbf{M_{IIA}}$ contain the actual peripheral shells for compounds **11**, **12** and **13** and model systems for the core fullerene as shown in Figures S10–S12. d1, d2, α and β parameters are defined in Figures 4 (caption) and S9. [b] $\mathbf{M_I}$ and $\mathbf{M_{II}}$ are the simplest models in which all the malonates are replaced by methylene units, except the ones that link the peripheral and core fullerenes. [c] Estimated radius for the corresponding theoretical model. [d] The two C_{60} models are built from the three C_{60} models by removing the linkers to the core fullerene. [e] Interaction energies at PM6 in kcal mol^{-1} correspond to E(two C_{60} model)-2E(C_{60}), where the two C_{60} model structures are reoptimized except for $\mathbf{M_I}$ and $\mathbf{M_{II}}$ entries. [f] All DFT energies were computed from PM6 geometries.

−40 and −115 kcal mol^{-1} (Table 3). The strength of the interaction depends directly on the distance between fullerenes and the number of interactions between them. Model $\mathbf{M_{IB}}$ shows same peripheral d_1 distance as non-functionalized fullerene $\mathbf{M_I}$, however the interaction energy is around −90 kcal mol^{-1}. Therefore, the length of the C_{60}-sugar spacer along with the presence of the three terminal saccharides allows the peripheral fullerenes to interact rather efficiently. The interaction takes place essentially through the hydrogen bonds established between hydroxyl groups of the sugars and the nitrogen atoms of the triazole ring (Figure 5). Somehow, these different interaction energy values define the compactness degree of the glycofullerene, making it more rigid or flexible depending on the strength of the interaction between fullerenes.[32]

To explore the interaction between pairs of fullerenes, some models with five C_{60} containing perpendicular pairs of peripheral fullerenes were also analysed (Figure S12). The results are analogous to those presented before. Interaction between fullerenes within the same pair, i.e., attached to the same cyclopropane ring, compression of structures and isosceles triangle disposition of fullerenes are reproduced.

Furthermore, we find that the interaction between axial and equatorial pairs of fullerenes is somewhat attractive (≈ −24 kcal mol^{-1}) for the model containing spacers II and A. If a larger C_{60}-C_{60} spacer is used, the interaction between two neighbouring adducts is essentially null. This means that shorter spacers induce a more compact globular glycofullerene because the pair of fullerenes are connected, i.e., able to interact, and they are not free as in the case of longer spacers (Figure S12).

In order to have a clearer visualization of the glycodendrimeric tridecafullerene, we constructed from the $\mathbf{M_{IIA}}$ model a complete structure for glycofullerene **13**, and then

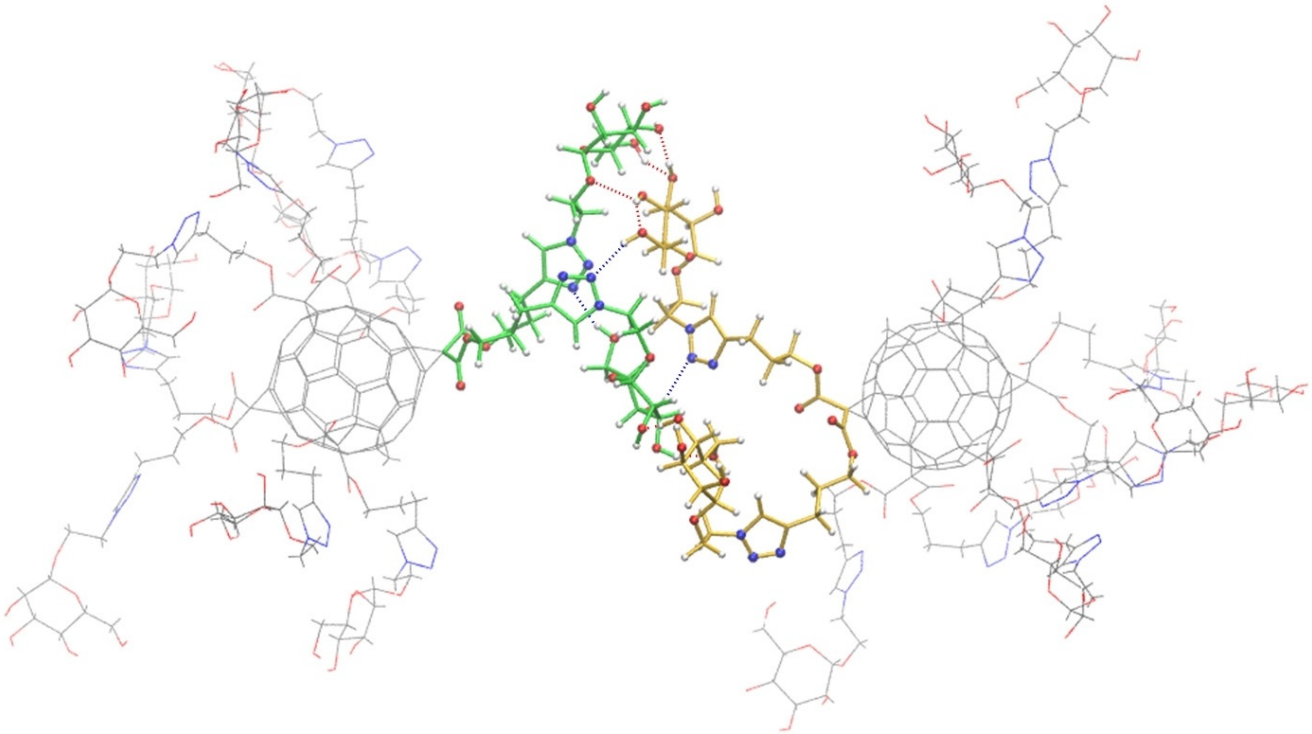

Figure 5. Optimized two C_{60} model corresponding to $\mathbf{M_{IIA}}$, highlighting the hydrogen bonds formed between fullerenes.

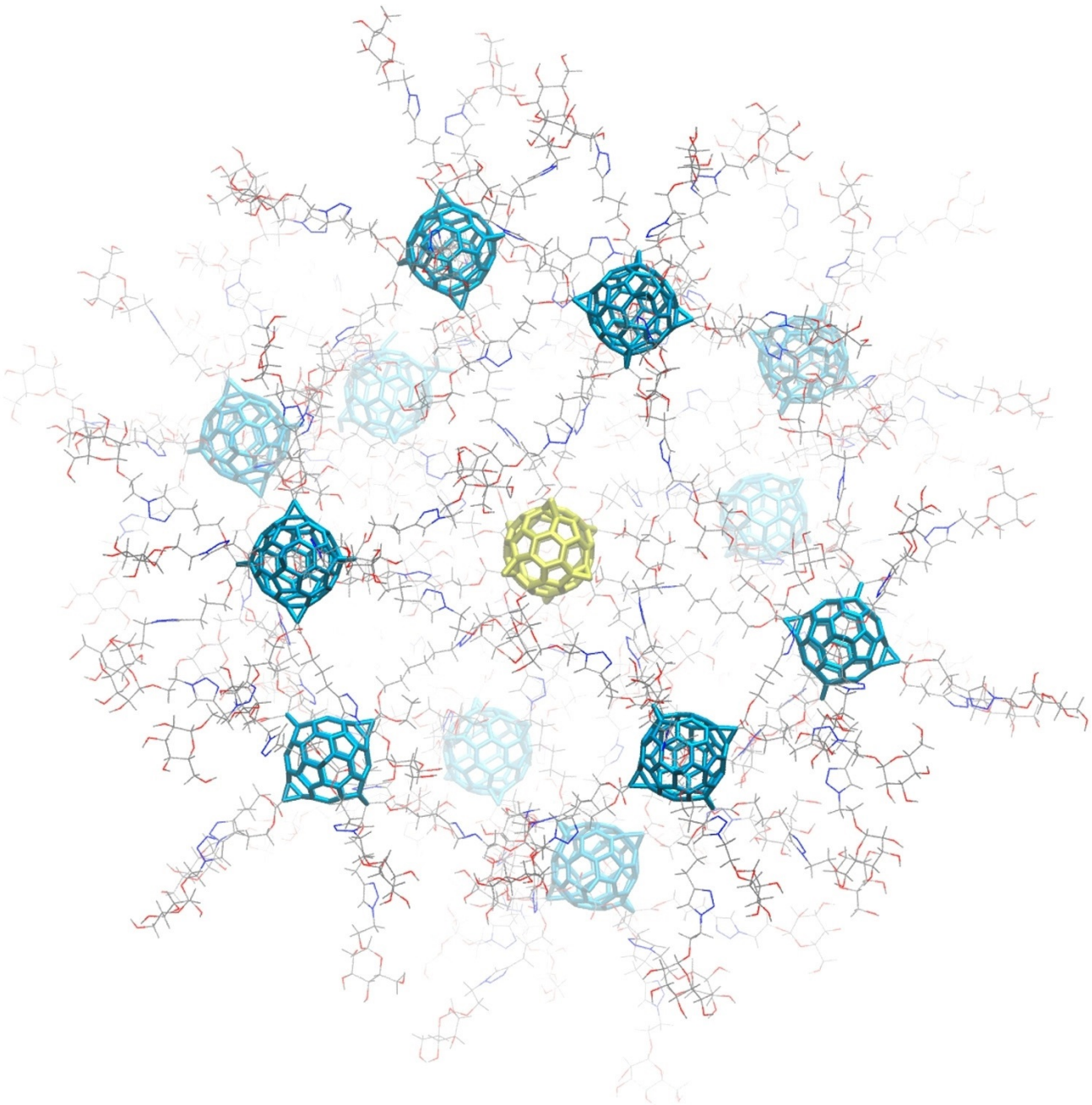

Figure 6. 3D representation for compound **13**. Core C_{60} in yellow. Interactions among saccharides make the system very compact for short C_{60}-C_{60} spacers.

it was partially relaxed. Figure 6 shows a 3D representation of the computed structure. Compound **13** is presumably quite fluxional given the composition and total number of atoms (7086), but the structure in Figure 6 clearly shows the compactness of this giant molecule, and the presence of interactions between pairs of neighboring fullerenes. It is also relevant to emphasize the *pseudo-spherical* layer that the sugars make up around the 12 peripheral C_{60}. Probably, this layer is the only part of the molecule that is in contact with the solvent in aqueous solution, while its inside is supposed to have a hydrophobic nature according to the results of the photophysical characterization.

Conclusion

The synthesis and photophysical behavior of a series of tridecafullerenes (a [60]fullerene core surrounded by a shell of twelve C_{60} units endowed with 120 or 360 mannoses and with different linkers) is reported. Triplet excited-state lifetimes of the tridecafullerenes in aqueous solution are strongly dependent on the type of linker between the fullerenes, and short alkyl chains afford structures with longer triplet lifetimes than those with larger polyether-like spacers. Moreover, triplet-state quenching experiments with O_2 and N_3^- anion suggest limited access of water molecules to the inner

domains of the tridecafullerenes, due to the interweaved chains with terminal sugars (H-bonding network) and the tightness provided, in particular, by the short alkyl-type spacers connecting the shell fullerenes to the central core unit. Consequently, the intersystem crossing efficiency and the triplet excited-state lifetimes (showing an unprecedented value as long as 93000 μs in the liquid phase at room temperature!) of the tridecafullerenes are modulated. Molecular modelling helps to ascertain the origin of the differences in the experimental photophysical properties of the giant superfullerenes in terms of the dissimilar structural compactness provided by sugars' shell and the highly hydrophobic nature of the short alkyl spacers among the core–shell C_{60} units.

The results now reported allow a better understanding of the structure and features of these singular systems, and pave the way to a fine control on the structural, biological and photophysical properties on these less-known but amazing globular-shape multivalent fullerenes. In particular, thanks to the ultra-long triplet lifetime exhibited by one of our tridecafullerenes and the quantitative quenching of this triplet by O_2, the complete trapping of the triplet state by oxygen, even in hypoxic environments, might find applications for the photodynamic treatment of hypoxic tumours. Further work is underway on the exploitation of compounds with ultra-long excited-state triplet lifetimes such as **13** in biomedicine, photovoltaics, photocatalysis, photon upconversion and other nonlinear phenomena like reverse saturable absorption under low irradiance.

Acknowledgements

Financial support by the Ministerio de Economía y Competitividad (MINECO) of Spain (projects CTQ2017-84327-P, CTQ2017-83531-R, CTQ2017-87269-P, CTQ2017-86265-P, CTQ2015-71896-REDT and CTQ2016-78454-C2-1-R) is acknowledged. J.M.P. also thanks the Generalitat de Catalunya for support (2017SGR629) and the ICREA foundation for an ICREA ACADEMIA award. K.A. thanks MINECO for a FPU fellowship. C.H. thanks the European Social Funds and the SUR del DEC de la Generalitat de Catalunya for his predoctoral fellowships (Grant No. 2017 FI_B 00617 and 2018 FI_B1 00174). IMDEA Nanoscience thanks support from the "Severo Ochoa" Programme for Centers of Excellence in R&D (MINECO, Grant SEV-2016-0686).

Conflict of interest

The authors declare no conflict of interest.

Keywords: fullerenes · glycoconjugates · photochemistry · triplet lifetime · triplet quenching

[1] a) J. M. Fernández-García, P. J. Evans, S. Filippone, M. A. Herranz, N. Martín, *Acc. Chem. Res.* **2019**, *52*, 1565 – 1574; b) N. Martín, *Adv. Energy Mater.* **2017**, *7*, 1601102; c) B. M. Illescas, J. Rojo, R. Delgado, N. Martín, *J. Am. Chem. Soc.* **2017**, *139*, 6018 – 6025; d) H. Liu, L. Zhang, M. Yan, J. Yu, *J. Mater. Chem. B* **2017**, *5*, 6437 – 6450; e) Z. Yang, J. Ren, Z. Zhang, X. Chen, G. Guan, L. Qiu, Y. Zhang, H. Peng, *Chem. Rev.* **2015**, *115*, 5159 – 5223.

[2] a) Y. Zhang, H. Zhang, Q. Zou, R. Xing, T. Jiao, X. Yan, *J. Mater. Chem. B* **2018**, *6*, 7335 – 7342; b) A. Insuasty, C. Atienza, J. L. López, J. Marco-Martínez, S. Casado, A. Saha, D. M. Guldi, N. Martín, *Sci. Rep.* **2015**, *5*, 14154; c) K. Minami, K. Okamoto, K. Doi, K. Harano, E. Noiri, E. Nakamura, *Sci. Rep.* **2014**, *4*, 4916.

[3] a) F. Leng, I. C. Gerber, P. Lecante, A. Bentaleb, A. Muñoz, B. M. Illescas, N. Martín, G. Melinte, O. Ersen, H. Martinez, M. R. Axet, P. Serp, *Chem. Eur. J.* **2017**, *23*, 13379 – 13386; b) J. Luczkowiak, A. Muñoz, M. Sánchez-Navarro, R. Ribeiro-Viana, A. Ginieis, B. M. Illescas, N. Martín, R. Delgado, J. Rojo, *Biomacromolecules* **2013**, *14*, 431 – 437.

[4] a) J. Ramos-Soriano, J. J. Reina, B. M. Illescas, N. de la Cruz, L. Rodríguez-Pérez, F. Lasala, J. Rojo, R. Delgado, N. Martín, *J. Am. Chem. Soc.* **2019**, *141*, 15403 – 15412; b) L. Rodríguez-Pérez, J. Ramos-Soriano, A. Pérez-Sánchez, B. M. Illescas, A. Muñoz, J. Luczkowiak, F. Lasala, J. Rojo, R. Delgado, N. Martín, *J. Am. Chem. Soc.* **2018**, *140*, 9891 – 9898; c) J. F. Nierengarten, *Chem. Commun.* **2017**, *53*, 11855 – 11868; d) A. Muñoz, D. Sigwalt, B. M. Illescas, J. Luczkowiak, L. Rodríguez-Pérez, I. Nierengarten, M. Holler, J. S. Remy, K. Buffet, S. P. Vincent, J. Rojo, R. Delgado, J. F. Nierengarten, N. Martín, *Nat. Chem.* **2016**, *8*, 50 – 57.

[5] F. Prat, C. Martí, S. Nonell, X. Zhang, C. S. Foote, R. González Moreno, J. L. Bourdelande, J. Font, *Phys. Chem. Chem. Phys.* **2001**, *3*, 1638 – 1643.

[6] a) A. Muñoz, B. M. Illescas, J. Luczkowiak, F. Lasala, R. Ribeiro-Viana, J. Rojo, R. Delgado, N. Martín, *J. Mater. Chem. B* **2017**, *5*, 6566 – 6571; b) A. Muñoz, B. M. Illescas, M. Sánchez-Navarro, J. Rojo, N. Martín, *J. Am. Chem. Soc.* **2011**, *133*, 16758 – 16761; c) H. Kato, C. Böttcher, A. Hirsch, *Eur. J. Org. Chem.* **2007**, 2659 – 2666.

[7] a) L. Shen, K. M. Cai, J. Yu, J. J. Cheng, *Bioconjugate Chem.* **2019**, *30*, 2317 – 2322.

[8] J. Wang, Y. Hang, J. Hua, *Sens. Actuators B* **2019**, *282*, 232 – 242.

[9] P. Yuan, Z. Ruan, T. Li, Y. Tian, Q. Cheng, L. Yan, *J. Mater. Chem. B* **2019**, *7*, 6770 – 6777.

[10] G. Cutrone, G. Benkovics, M. Malanga, J. M. Casas-Solvas, E. Fenyvesi, S. Sortino, L. García-Fuentes, A. Vargas-Berenguel, *Carbohydr. Polym.* **2018**, *199*, 649 – 660.

[11] X. Gao, D. Mao, X. Zuo, F. Hu, J. Cao, P. Zhang, J. Z. Sun, J. Liu, B. Liu, B. Z. Tang, *Anal. Chem.* **2019**, *91*, 6836 – 6843.

[12] a) M. Montalti, A. Credi, L. Prodi, M. T. Gandolfi, *Handbook of Photochemistry*, 3rd ed., CRC, Boca Raton, FL, **2006**, chap. 3, Table 3a, pp. 83 – 156; b) M. Montalti, A. Credi, L. Prodi, M. T. Gandolfi, *Handbook of Photochemistry*, 3rd ed., CRC, Boca Raton, FL, **2006**, chap. 5, Table 5a, pp. 378 – 404; c) A. A. Rachford, S. Goeb, R. Ziessel, F. N. Castellano, *Inorg. Chem.* **2008**, *47*, 4348 – 4355; d) S. Ji, W. Wu, W. Wu, H. Guo, J. Zhao, *Angew. Chem. Int. Ed.* **2011**, *50*, 1626 – 1629; *Angew. Chem.* **2011**, *123*, 1664 – 1667; e) M. Canlica, T. Nyokong, *Dalton Trans.* **2011**, *40*, 5285 – 5290; f) W. Wu, W. Wu, S. Ji, H. Guo, J. Zhao, *Dalton Trans.* **2011**, *40*, 5953 – 5963; g) Y. Liu, W. Wu, J. Zhao, X. Zhang, H. Guo, *Dalton Trans.* **2011**, *40*, 9085 – 9089; h) L. Huang, L. Zeng, H. Guo, W. Wu, W. Wu, S. Ji, J. Zhao, *Eur. J. Inorg. Chem.* **2011**, 4527 – 4533; i) J. Zhao, S. Ji, W. Wu, W. Wu, H. Guo, J. Sun, H. Sun, Y. Liu, Q. Li, L. Huang, *RSC Adv.* **2012**, *2*, 1712 – 1728; j) L. Ma, S. Guo, J. Sun, C. Zhang, J. Zhao, H. Guo, *Dalton Trans.* **2013**, *42*, 6478 – 6488; k) W. Wu, L. Liu, X. Cui, C. Zhang, J. Zhao, *Dalton Trans.* **2013**, *42*, 14374 – 14379; l) X. Jiang, J. Peng, J. Wang, X. Guo, D. Zhao, Y. Ma, *ACS Appl. Mater. Interfaces* **2016**, *8*, 3591 – 3600; m) C. Wang, L. Lystrom, H. Yin, M. Hetu, S. Kilina, S. A. McFarland, W. Sun, *Dalton Trans.* **2016**,

45, 16366 – 16378; n) J. E. Yarnell, A. Chakraborty, M. Myahkostupov, K. M. Wright, F. N. Castellano, *Dalton Trans.* **2018**, *47*, 15071 – 15081; o) D. J. Stewart, J. Shi, T. R. Naranjo, T. A. Grusenmeyer, J. M. Artz, C. L. McCleese, R. M. O'Donnell, T. M. Cooper, W. M. Shensky III, J. E. Haley, *Phys. Chem. Chem. Phys.* **2018**, *20*, 28412 – 28418; p) L. Jiao, F. Song, J. Cui, X. Peng, *Chem. Commun.* **2018**, *54*, 9198 – 9201; q) M. Byrdin, C. Duan, D. Bourgeois, K. Brettel, *J. Am. Chem. Soc.* **2018**, *140*, 2897 – 2905; r) S. Treiling, C. Wang, C. Förster, F. Reichenauer, J. Kalmbach, P. Boden, J. P. Harris, L. M. Carrella, E. Rentschler, U. Resch-Genger, C. Reber, M. Seitz, M. Gerhards, K. Heinze, *Angew. Chem. Int. Ed.* **2019**, *58*, 18075 – 18085; *Angew. Chem.* **2019**, *131*, 18243 – 18253; s) L. Wang, S. Monro, P. Cui, H. Yin, B. Liu, C. G. Cameron, W. Xu, M. Hetu, A. Fuller, S. Kilina, S. A. McFarland, W. Sun, *ACS Appl. Mater. Interfaces* **2019**, *11*, 3629 – 3644; t) Y. Hou, Q. Liu, J. Zhao, *Chem. Commun.* **2020**, *56*, 1721 – 1724; u) Z. Mahmood, N. Rehmat, S. Ji, J. Zhao, S. Sun, M. Di Donato, M. Li, M. Teddei, Y. Huo, *Chem. Eur. J.* **2020**, *26*, 14912 – 14918; v) Y. Dong, B. Dick, J. Zhao, *Org. Lett.* **2020**, *22*, 5535 – 5539; w) Y. Dong, A. Elmali, J. Zhao, B. Dick, A. Karatay, *ChemPhysChem* **2020**, *21*, 1388 – 1401; x) Y. Hou, J. Liu, N. Zhang, J. Zhao, *J. Phys. Chem. A* **2020**, *124*, 9360 – 9374; y) H. Li, S. Liu, L. Lystrom, S. Kilina, W. Sun, *J. Photochem. Photobiol. A* **2020**, *400*, 112609.

[13] a) H. Li, S. A. Haque, A. Kitaygorodskiy, M. J. Meziani, M. Torres-Castillo, Y. P. Sun, *Org. Lett.* **2006**, *8*, 5641 – 5643; b) I. Lamparth, C. Maichle-Mössmer, A. Hirsch, *Angew. Chem. Int. Ed. Engl.* **1995**, *34*, 1607 – 1609; *Angew. Chem.* **1995**, *107*, 1755 – 1757.

[14] a) I. Nierengarten, J. F. Nierengarten, *Chem. Rec.* **2015**, *15*, 31 – 51; b) V. V. Rostovtsev, L. G. Green, V. V. Fokin, K. B. Sharpless, *Angew. Chem. Int. Ed.* **2002**, *41*, 2596 – 2599; *Angew. Chem.* **2002**, *114*, 2708 – 2711.

[15] H. Isobe, K. Cho, N. Solin, D. B. Werz, P. H. Seeberger, E. Nakamura, *Org. Lett.* **2007**, *9*, 4611 – 4614.

[16] J. F. Nierengarten, J. Iehl, V. Oerthel, M. Holler, B. M. Illescas, A. Muñoz, N. Martín, J. Rojo, M. Sánchez-Navarro, S. Cecioni, S. Vidal, K. Buffet, M. Durka, S. P. Vincent, *Chem. Commun.* **2010**, *46*, 3860 – 3862.

[17] a) J. Iehl, T. L. A. Nguyen, S. Frein, U. Hahn, J. Barberá, J. F. Nierengarten, R. Deschenaux, *Liq. Cryst.* **2017**, *44*, 1852 – 1860; b) D. Sigwalt, R. Caballero, M. Holler, J. M. Strub, A. Van Dorsselaer, J. F. Nierengarten, *Eur. J. Org. Chem.* **2016**, 2882 – 2887; c) J. Li, L. C. Nye, L. K. Wasserthal, C. Vinh, R. W. Kirschbaum, I. Ivanović-Burmazović, A. Hirsch, T. Drewello, *Eur. J. Org. Chem.* **2015**, 2282 – 2290; d) S. Campidelli, T. Brandmüller, A. Hirsch, I. M. Saez, J. W. Goodby, R. Deschenaux, *Chem. Commun.* **2006**, 4282 – 4284; e) F. Prat, R. Stackow, R. Bernstein, W. Qian, Y. Rubin, C. S. Foote, *J. Phys. Chem. A* **1999**, *103*, 7230 – 7235; f) L. Isaacs, F. Diederich, R. F. Haldimann, *Helv. Chim. Acta* **1997**, *80*, 317 – 342.

[18] D. M. Guldi, M. Prato, *Acc. Chem. Res.* **2000**, *33*, 695 – 703.

[19] a) K. E. van Holde, W. C. Johnson, P. S. Ho, *Principles of Physical Biochemistry*, Pearson-Prentice Hall, Upper Saddle River, **2005**, chap. 9; b) D. García-Fresnadillo, O. Lentzen, I. Ortmans, E. Defrancq, A. Kirsch-De Mesmaeker, *Dalton Trans.* **2005**, 852 – 856.

[20] O. Shimizu, J. Watanabe, K. Imakubo, S. Naito, *Chem. Lett.* **1999**, *28*, 67 – 68.

[21] D. García-Fresnadillo, N. Boutonnet, S. Schumm, C. Moucheron, A. Kirsch-De Mesmaeker, E. Defrancq, J. F. Constant, J. Lhomme, *Biophys. J.* **2002**, *82*, 978 – 987.

[22] R. F. Enes, A. C. Tomé, J. A. S. Cavaleiro, A. El-Agamey, D. J. McGarvey, *Tetrahedron* **2005**, *61*, 11873 – 11881.

[23] a) M. R. Wasielewski, M. P. O'Neill, K. R. Lykke, M. J. Pellin, D. M. Gruen, *J. Am. Chem. Soc.* **1991**, *113*, 2774 – 2776; b) L. Akselrod, H. J. Byrne, C. Thomsen, A. Mittelbach, S. Roth, *Chem. Phys. Lett.* **1993**, *212*, 384 – 390; c) V. N. Denisov, B. N. Mavrin, A. A. Zakhidov, G. Ruani, R. Zamboni, C. Taliani, *Synth. Met.* **1993**, *56*, 3119 – 3214; d) D. J. van den Heuvel, I. Y. Chan, E. J. J. Groenen, J. Schmidt, G. Meijer, *Chem. Phys. Lett.* **1994**, *231*, 111 – 118; e) A. Sassara, G. Zerza, M. Chergui, *Chem. Phys. Lett.* **1996**, *261*, 213 – 220.

[24] C. Dyer-Smith, L. X. Reynolds, A. Bruno, D. D. C. Bradley, S. A. Haque, J. Nelson, *Adv. Funct. Mater.* **2010**, *20*, 2701 – 2708.

[25] G. Schick, M. Levitus, L. Kvetko, B. A. Johnson, I. Lamparth, R. Lunkwitz, B. Ma, S. I. Khan, M. A. Garcia-Garibay, Y. Rubin, *J. Am. Chem. Soc.* **1999**, *121*, 3246 – 3247.

[26] R. R. Hung, J. J. Grabowski, *J. Phys. Chem.* **1991**, *95*, 6073 – 6075.

[27] M. Montalti, A. Credi, L. Prodi, M. T. Gandolfi, *Handbook of Photochemistry*, 3rd ed., CRC, Boca Raton, FL, **2006**, chap. 6, Table 6a, p. 424.

[28] D. García-Fresnadillo, S. Lacombe, in *Singlet Oxygen: Applications in Biosciences and Nanosciences*, *Vol. 1* (Eds.: S. Nonell, C. Flors), The Royal Society of Chemistry, Cambridge, **2016**, pp. 105 – 143.

[29] a) C. Reichardt, *Solvents and Solvent Effects in Organic Chemistry*, 3rd ed., Wiley-VCH, Weinheim, **2003**; b) D. A. Samuels, R. B. Weisman, *Chem. Phys. Lett.* **1998**, *295*, 105 – 112; c) F. A. Salazar, A. Fedorov, M. N. Berberan-Santos, *Chem. Phys. Lett.* **1997**, *271*, 361 – 366.

[30] a) M. B. Ballatore, M. B. Spesia, M. E. Milanesio, E. N. Durantini, *RSC Adv.* **2018**, *8*, 22876 – 22886; b) R. Yin, M. Wang, Y. Y. Huang, G. Landi, D. Vecchio, L. Y. Chiang, M. R. Hamblin, *Free Radical Biol. Med.* **2015**, *79*, 14 – 27.

[31] T. Chachibaia, M. Martin Pastor, *C. J. Car. Res.* **2017**, *3*, 13.

[32] A. Kraft, M. Gsänger, F. Beuerle, *Eur. J. Org. Chem.* **2014**, 523 – 528.

Manuscript received: March 25, 2021
Revised manuscript received: April 27, 2021
Accepted manuscript online: May 13, 2021
Version of record online: June 14, 2021

